Supplementary material to:

Oxidative potential in rural, suburban and city centre atmospheric environments in Central Europe

Máté VÖRÖSMARTY[1], Gaëlle UZU[2], Jean-Luc JAFFREZO[2], Pamela DOMINUTTI[2], Zsófia KERTÉSZ[3], Enikő PAPP[3], and Imre SALMA[4]

[1] Hevesy György Ph. D. School of Chemistry, Eötvös Loránd University, Budapest, Hungary
[2]University of Grenoble Alps, IRD, CNRS, INRAE, Grenoble, France
[3] Laboratory for Heritage Science, Institute for Nuclear Research, Debrecen, Hungary
[4] Institute of Chemistry, Eötvös Loránd University, Budapest, Hungary

Correspondence to: Imre Salma (salma.imre@ttk.elte.hu)

S1 In situ measurements and data

Concentrations of NO/NO_x(=$NO+NO_2$), CO, O_3 and SO_2 were obtained from the Hungarian Air Quality Network (Salma et al., 2020a). They were determined by chemiluminescence (Thermo 42C), IR absorption (Thermo 48i), UV absorption (Ysselbach 49C) and UV fluorescence (Ysselbach 43C) methods, respectively with a time resolution of 1 h. In the rural background and suburban area, the concentrations were obtained directly at the sampling locations. In the city centre, the pollutants were measured in 4.5 km in the upwind prevailing direction from the sampling site.

In the city centre, particle number size distributions were also determined by a flow-switching-type differential mobility size spectrometer in a diameter range from 6 to 1000 nm in 30 channels in the dry state of particles with a time resolution of 8 min (Salma et al., 2016). Concentrations in several size fractions were calculated. Of them, the daily mean concentrations of the total particles ($N_{6–1000}$) and of particles in the diameter range of 25–100 nm ($N_{25–100}$) were used here. The latter concentration is often associated with emission sources from vehicles (Salma et al., 2020b).

Local air temperature (T) and relative humidity (RH) data were acquired by standardised meteorological methods (anemometer HD52.3D17, Delta OHM, Italy or Vaisala HMP45D and Vaisala WAV15A, Finland) on sites with a time resolution of 1 min (Salma et al., 2022).

Table S1. Ranges and averages of the daily concentrations for NO, NO_2, CO, O_3 and SO_2 (all in µg m^{-3}), for total particle numbers ($N_{6–1000}$) and particles in the diameter range of 25–100 nm ($N_{25–100}$, both in $\times 10^3$ cm^{-3}) and of air temperature (T,°C) and relative humidity (RH, %) in the rural background, suburban area and city centre. The average is median for the concentrations and mean for the meteorological data.

Site/ Variable	Rural background			Suburban area			City centre		
	Minimum	Average	Maximum	Minimum	Average	Maximum	Minimum	Average	Maximum
NO	–			0.3	1.8	50	6	20	96
NO_2	–			5	20	64	24	41	62
CO	–			218	681	1071	282	579	785
O_3	10	85	115	1	42	92	1	17	73
SO_2	–			0.7	1.8	4.1	2.5	5.1	7.3
$N_{6–1000}$	–	–	–	–	–	–	3.8	11.5	21
$N_{25–100}$	–	–	–	–	–	–	1.53	4.2	10.3
T	–3.0	12	25	–2.6	14	27	–1.7	15	25
RH	51	80	97	38	65	89	38	68	86

S2 Details of aerosol source interpretation

The interpretation of the factors derived by the PMF modelling was based on the presence and amounts of their marker chemical species, on the tendencies in the time series of the factor intensities, on the crustal enrichment factors (Table S2; e.g. Salma and Maenhaut, 2006), and on the correlations with selected variables and the other sources (Table S3).

The BB source was identified by high shares of LVG, K, EC, OC and Rb (Fig. S1). It also contained Cl, Br, Zn and Pb, which could originate from agricultural-waste and household-waste burnings, including (illegal) burnings of some solid materials such as plastics, furniture, fibreboards, tyres and coloured paper together with biomass (Hoffer et al., 2021). Its intensity was the largest in winter, substantial in autumn and very low in spring and summer. The intensity of the BB source resulted in the largest significant and positive coefficient of correlations (0.97–0.99) with EC_{BB} and OC_{BB} at all sites and they were also large and significant with $PM_{2.5}$ mass. Its correlations with O_3 were significant and negative due to the seasonal tendencies of BB and O_3 and to additional common factors governing them.

The suspended dust source showed the largest contributions from crustal elements such as Ti, Ca, and Fe (Fig. S2). At the rural location, it was virtually fugitive mineral and soil dust made of geogenic elements. In the urban sites, the dust also comprised further constituents including S (mainly anthropogenic according to its crustal EF in Table S2), V (partly anthropogenic), EC, OC, Ba (partly anthropogenic) and Br (mainly anthropogenic). The effect of the Saharan dust intrusion into the Carpathian Basin on 15 April

2018 showed up evidently and with extremely high source intensities at each location. The intensity of the dust source in the rural background was considerable in spring and summer (dryer or arid time periods), and low in winter and autumn. The agricultural activity contributed to the seasonal character as well. The intensity of the suspended dust source in the urban sites was less dependent on season. This can be explained by the increasing importance of traffic-blown dust to wind-blown dust. At these locations, construction activities can also produce fugitive dust enriched in Ca and Mg. Suspended dust anticorrelated significantly with the BB in the rural background and suburban area due to their seasonal tendencies (e.g. land surface areas are often wet or covered with snow in winter and autumn when BB is intensive).

Table S2. Mean crustal enrichment factors for the apportioned elemental concentrations in the suspended dust source for $PM_{2.5}$ size fraction relative to the average upper continental crustal rock composition with Ti as the lithogenic reference element separately in the rural background, suburban area and city centre.

Site/ Element	Rural background	Suburban area	City centre
S	–	1729	1388
Ca	2.5	3.7	4.4
V	–	4.3	3.8
Mn	–	2.8	2.9
Fe	1.0	1.9	2.1
Br	–	456	471
Ba	–	4.6	5.0
Pb	–	–	251

The road traffic source exhibited large contributions of EC, OC, Zn, Br, Mn, Cl, V, Ca, Ba, Pb, Cu and Fe (Fig. S3). Its intensity was basically balanced over the year. It also showed monotonic increase in the intensity from the rural background through the suburban area to the city centre. It exhibited strong and significant correlations with NO, NO_x and CO at the urban sites. Its coefficients of correlation with $N_{6–1000}$ (0.74), $N_{25–100}$ (0.81) and metal wear factor (0.77) were significant in the city centre.

The oil combustion source comprised large contributions of V, S, Mn, OC, Ni and Rb (Fig. S4). Its intensity was fairly constant over the whole year. It significantly correlated with the dust source in the rural background and suburban area (R=0.55 and 0.32, respectively) and with the SOC (0.68) in the city centre. It cannot be fully excluded that the oil combustion was partly mixed with coal combustion due to their collinearity caused by meteorological conditions in winter (Sect. 3.5).

The metal wear of vehicles was related to primary aerosol particles containing large contributions of Cr, Cu, Fe, Ni, Ba, Mn and Pb (Fig. S5). Its source intensity was balanced over the year at each location and followed that of road vehicle traffic. It showed no significant correlation in the rural background, while it correlated significantly and positively with vehicle traffic (R=0.77) and mixed industrial source (0.67) in the city centre. In the urban locations, it also exhibited significant positive correlations with SO_2, NO, CO, $N_{6–1000}$ and $N_{25–100}$. They all suggested that this source could be another statistical realisation or consequence of road traffic.

The last factor contained large contributions from Zn and also involved considerable shares of Ni, Pb, Cl and Ba (Fig. S6). Its source intensity was fairly balanced over the year at each location. At the urban cites, it correlated significantly and positively with SO_2, OC_{FF} and EC_{FF}. It cannot be completely excluded that its separate appearance was fostered by a few samples containing high concentrations of Zn. At the same time, it showed no significant correlation in the rural background. Therefore, it was interpreted as a mixed industrial source.

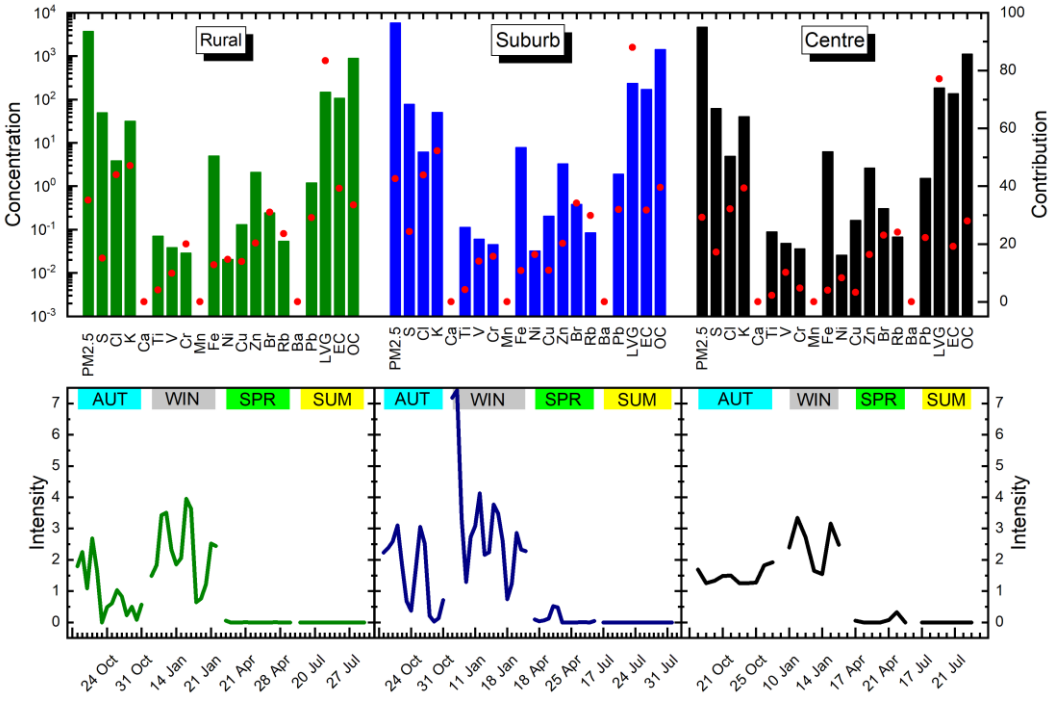

Figure S1. Concentrations of aerosol constituents (factor profiles, in ng m^{-3}; top panels, column bars) assigned to biomass burning source, mean contributions of this factor to total concentrations (in %; top panels, red dots) and time series of the factor intensity (bottom panels) separately for rural background, suburban area and city centre. The seasons are indicated on the bottom panels.

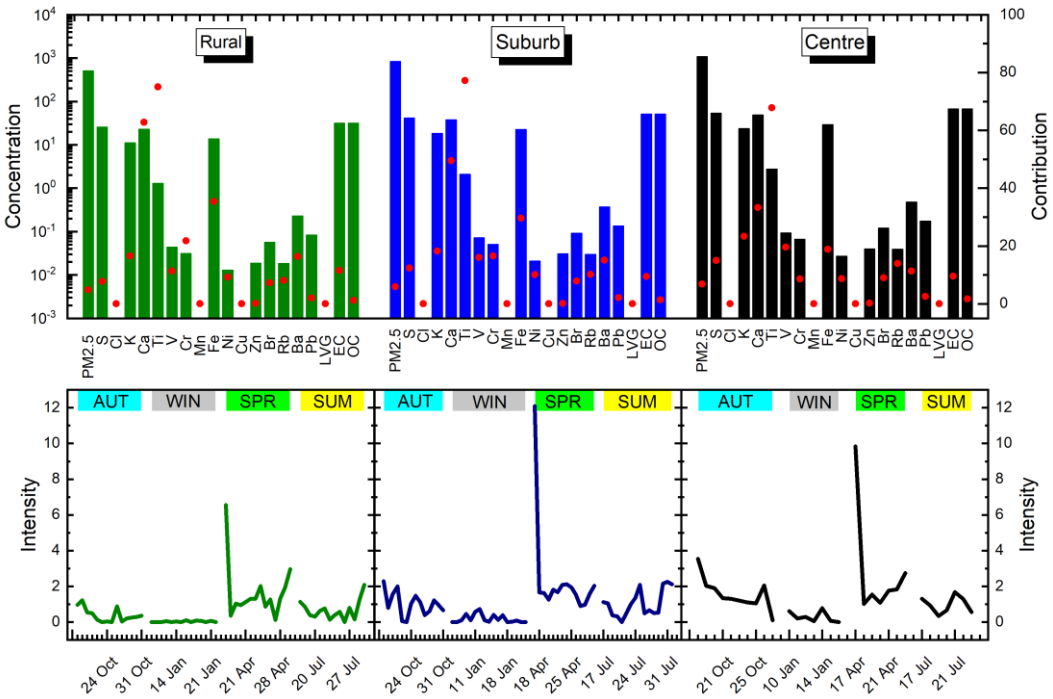

Figure S2. Concentrations of aerosol constituents (factor profiles, in ng m^{-3}; top panels, column bars) assigned to suspended dust source, mean contributions of this factor to total concentrations (in %; top panels, red dots) and time series of the factor intensity (bottom panels) separately for rural background, suburban area and city centre. The seasons are indicated on the bottom panels.

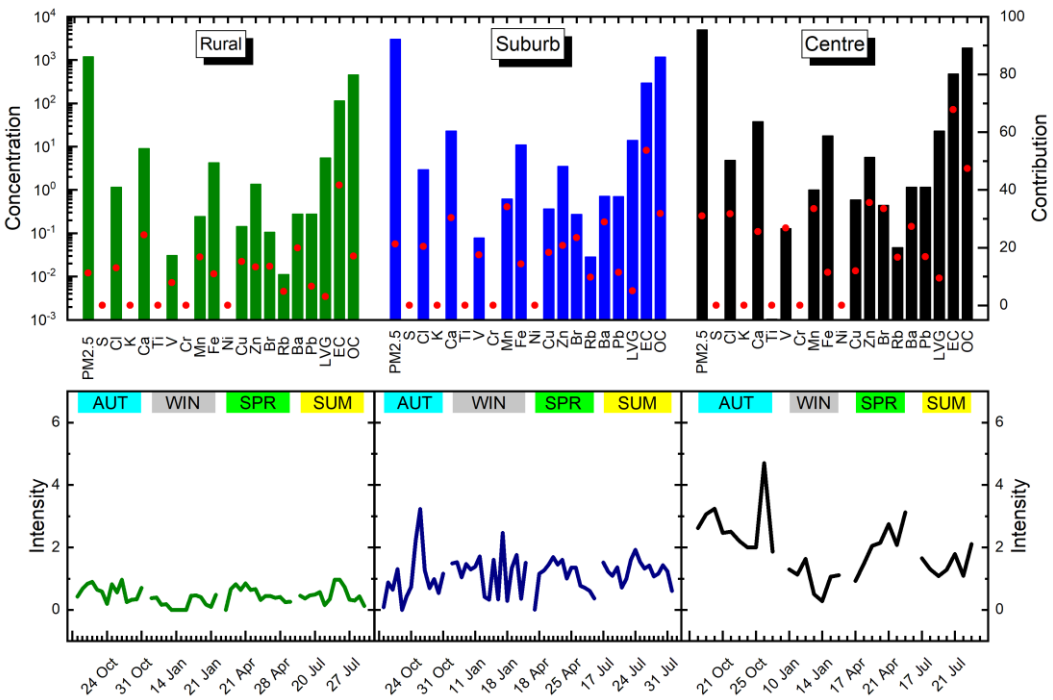

Figure S3. Concentrations of aerosol constituents (factor profiles, in ng m^{-3}; top panels, column bars) assigned to road traffic source, mean contributions of this factor to total concentrations (in %; top panels, red dots) and time series of the factor intensity (bottom panels) separately for city centre, suburban area and rural background. The seasons are indicated on the bottom panels.

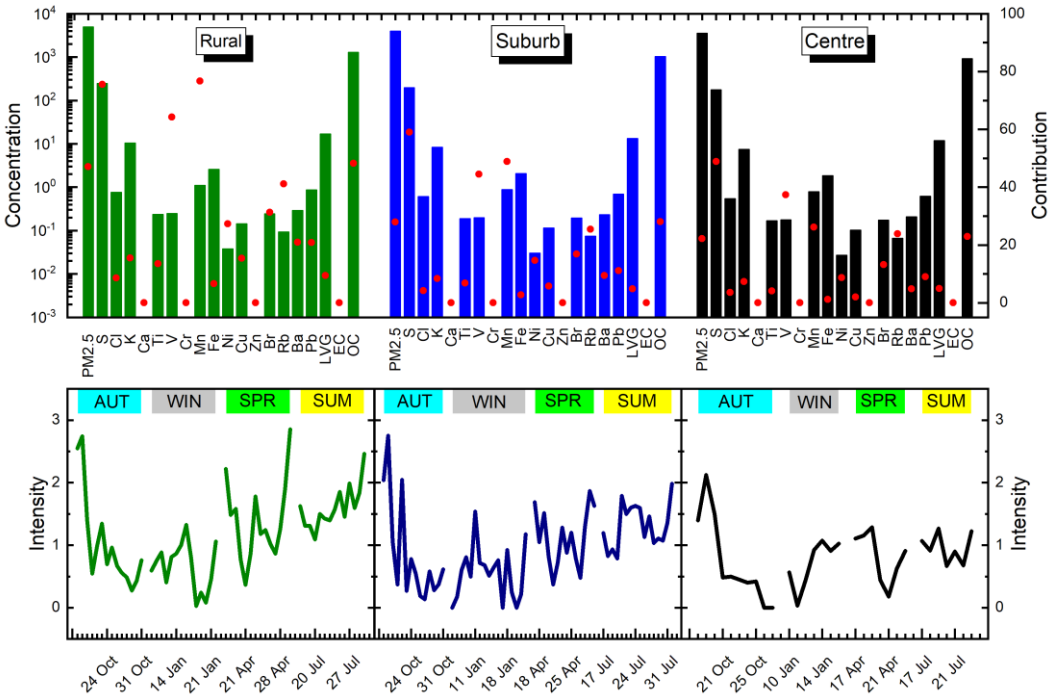

Figure S4. Concentrations of aerosol constituents (factor profiles, in ng m^{-3}; top panels, column bars) assigned to residual oil combustion source, mean contributions of this factor to total concentrations (in %; top panels, red dots) and time series of the factor intensity (bottom panels) separately for rural background, suburban area and city centre. The seasons are indicated on the bottom panels.

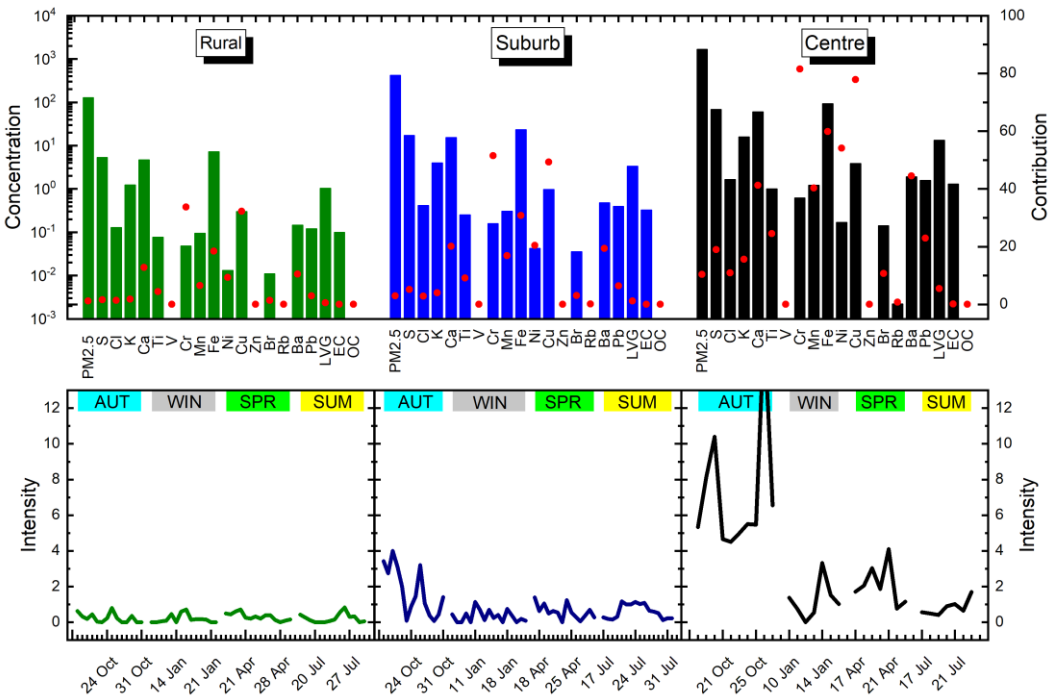

Figure S5. Concentrations of aerosol constituents (factor profile, in ng m^{-3}; top panels, column bars) assigned to vehicle metal wear, mean contributions of this factor to total concentrations (in %; top panels, red dots) and time series of the factor intensity (bottom panels) separately for city centre, suburban area and rural background. The seasons are indicated on the bottom panels.

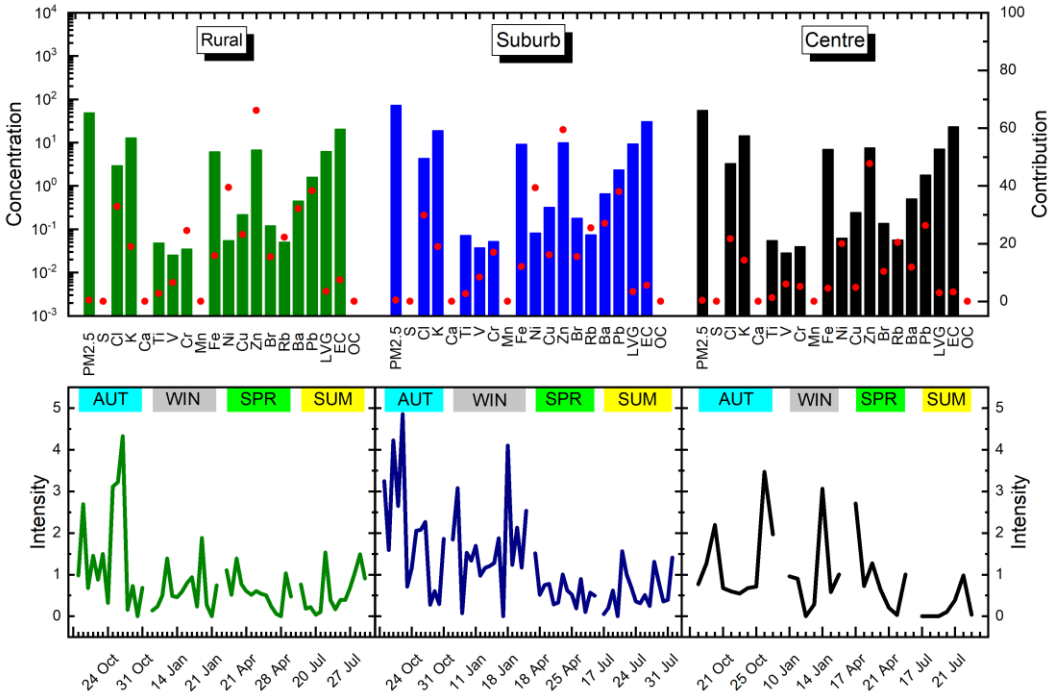

Figure S6. Concentrations of aerosol constituents (factor profile, in ng m^{-3}; top panels, column bars) assigned to mixed industrial source, mean contributions of this factor to total concentrations (in %; top panels, red dots) and time series of the factor intensity (bottom panels) separately for rural background, suburban area and city centre. The seasons are indicated on the bottom panels.

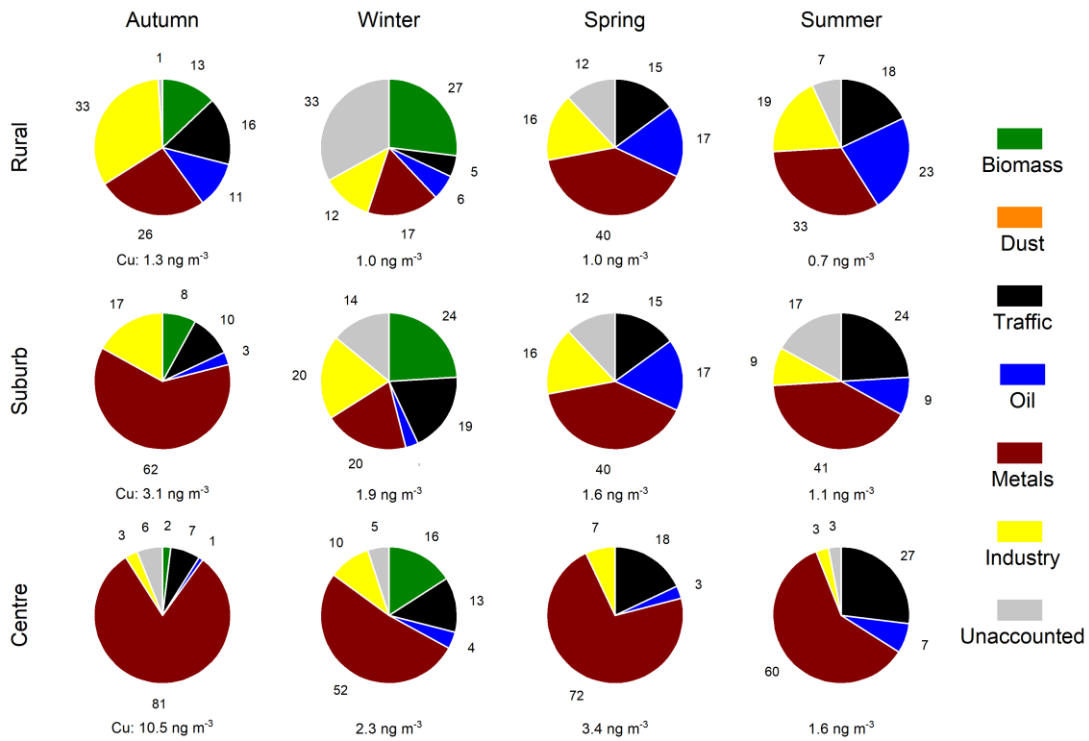

Figure S7. Mean contributions of biomass burning, suspended dust, road traffic, oil combustion, vehicle metal wear, mixed industrial source and unaccounted sources to atmospheric concentration of Cu (in %) as derived by PMF modelling in the rural background, suburban area and city centre in different seasons. The median atmospheric concentrations are shown under the circle charts.

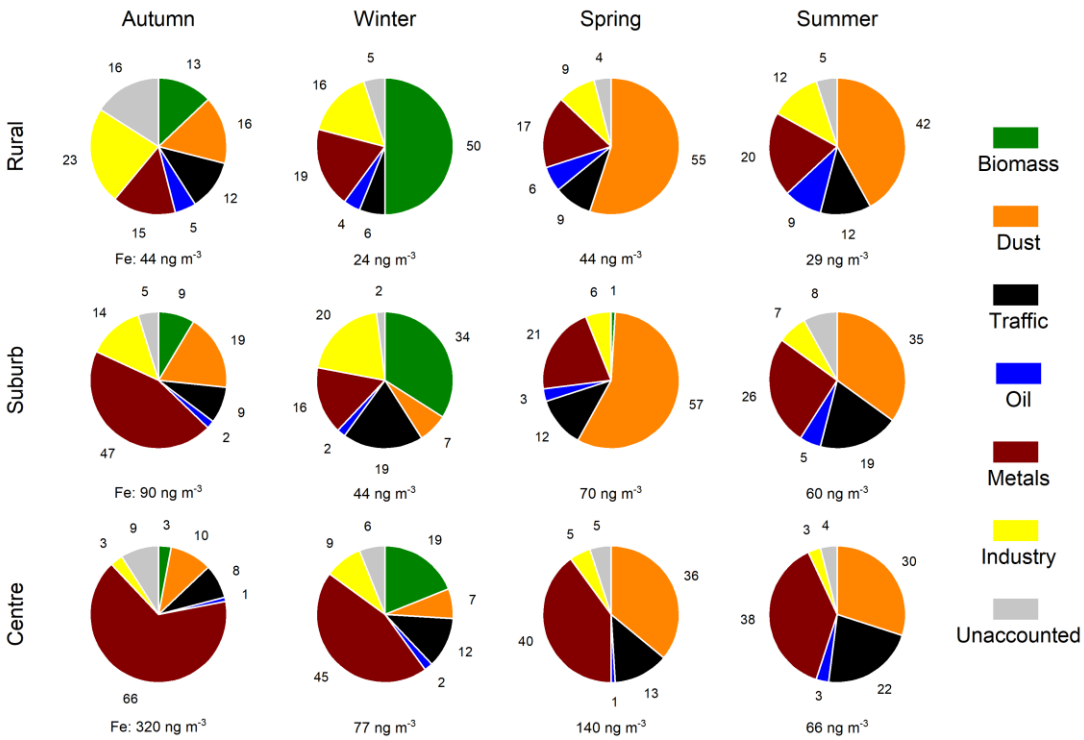

Figure S8. Mean contributions of biomass burning, suspended dust, road traffic, oil combustion, vehicle metal wear, mixed industrial source and unaccounted sources to atmospheric concentration of Fe (in %) as derived by PMF modelling in the rural background, suburban area and city centre in different seasons. The median atmospheric concentrations are shown under the circle charts.

S3 Correlations of oxidative potential with main aerosol sources and secondary organic carbon

Table S3. Pearson's coefficients of correlation between the oxidative potential (OP) determined by AA and DTT assays normalised to $PM_{2.5}$ mass (*m*; $OP_{AA,m}$ and $OP_{DTT,m}$, respectively, in nmol min^{-1} μg^{-1}) on the one side and the identified main aerosol sources of biomass burning, suspended dust, road traffic, oil combustion, vehicle metal wear and mixed industrial source on the other side in the rural background, suburban area and city centre. The significance of the correlations was evaluated by Student's t-test at a confidence level of p=0.05. The total number of samples is denoted by *n*. The nonsignificant correlations are indicated in Italic font.

Source Site, variable	Biomass burning	Suspended dust	Road traffic	Oil combustion	Metal wear	Industrial source
Rural background (n=56)						
$OP_{AA,V}$	0.88	*–0.21*	*–0.22*	*–0.13*	*0.04*	*0.08*
$OP_{DTT,V}$	0.39	*–0.07*	*–0.06*	*0.27*	*–0.16*	*0.07*
Suburban area (n=59)						
$OP_{AA,V}$	0.94	–0.30	0.27	–0.31	*0.12*	0.53
$OP_{DTT,V}$	0.60	*–0.17*	*–0.15*	*0.21*	0.37	0.55
City centre (n=28)						
$OP_{AA,V}$	0.85	*–0.14*	*0.30*	*–0.30*	0.55	*0.42*
$OP_{DTT,V}$	0.63	*–0.03*	0.47	*–0.12*	0.64	*0.42*

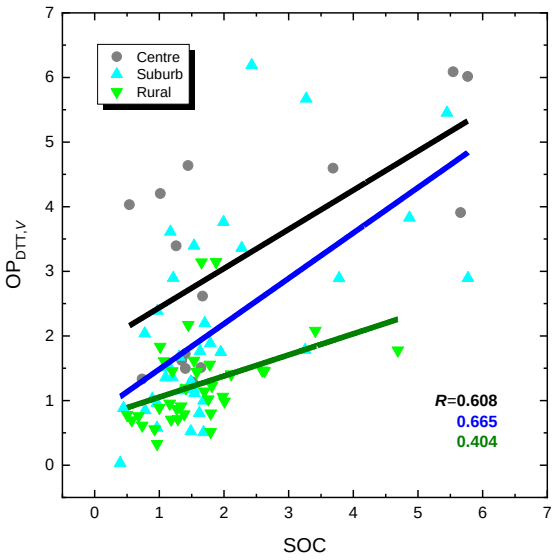

Figure S9. Scatter plots of oxidative potential (OP) determined by DTT assay and normalised to sampled air volume (*V*; $OP_{DTT,V}$, in unit of nmol min^{-1} m^{-3}) and secondary organic carbon (SOC, μg m^{-3}) for the rural background, suburban area and city centre. The lines represent linear regressions of the corresponding data points. The coefficients of correlation (*R*s) are also indicated. The slopes and SDs of the regression lines are 0.33±0.12, 0.70±0.16 and 0.61±0.19 nmol min^{-1} μg^{-1}, respectively.

S4 Results of multiple linear regression with the weighted least squares approach

Table S4. Slopes and intersects of the multiple linear regression with weighted least squares approach between oxidative potential (OP) determined by AA and DTT assays and normalised to sampled air volume ($OP_{AA,V}$ and $OP_{DTT,V}$, respectively) and the main aerosol sources of biomass burning, suspended dust, road traffic, oil combustion, vehicle metal wear and mixed industrial source in the rural background, suburban area and city centre. The number of samples available (*n*) and the coefficients of determination (R^2) are also shown.

Location/	Rural background		Suburban area		City centre	
Main source	$OP_{AA,V}$	$OP_{DTT,V}$	$OP_{AA,V}$	$OP_{DTT,V}$	$OP_{AA,V}$	$OP_{DTT,V}$
Biomass burning	1.4914	0.7368	1.1736	0.6458	1.0706	0.8038
Suspended dust	0.1762	–0.2476	0.6133	0.0135	0.0590	0.1644
Road traffic	1.2715	0.7602	–0.6832	0.2339	0.2885	0.8064
Oil combustion	0.3204	0.8804	0.8645	1.1057	–0.5084	0.5859
Vehicle metal wear	–0.0678	–1.2883	–0.3273	–0.1406	0.0467	0.1381
Mixed industrial	–0.3125	0.2660	0.1323	0.1341	0.0548	–0.3125
Intersect	–0.1825	–0.2233	0.1064	–0.5986	0.4075	–0.3698
N	52	51	56	55	28	28
R^2	0.982	0.948	0.862	0.801	0.906	0.854

References

Hoffer, A., Tóth, Á., Jancsek-Turóczi, B., Machon, A., Meiramova, A., Nagy, A., Marmureanu, L., and Gelencsér, A.: Potential new tracers and their mass fraction in the emitted PM_{10} from the burning of household waste in stoves, Atmos. Chem. Phys., 21, 17855–17864, https://doi.org/10.5194/acp-21-17855-2021, 2021.

Salma, I. and Maenhaut, W.: Changes in chemical composition and mass of atmospheric aerosol pollution between 1996 and 2002 in a Central European city, Environ. Pollut., 143, 479–488, https://doi.org/10.1016/j.envpol.2005.11.042, 2006.

Salma, I., Németh, Z., Weidinger, T., Kovács, B., and Kristóf, G.: Measurement, growth types and shrinkage of newly formed aerosol particles at an urban research platform, Atmos. Chem. Phys., 16, 7837–7851, https://doi.org/10.5194/acp-16-7837-2016, 2016.

Salma, I., Vasanits-Zsigrai, A., Machon, A., Varga, T., Major, I., Gergely, V., and Molnár, M.: Fossil fuel combustion, biomass burning and biogenic sources of fine carbonaceous aerosol in the Carpathian Basin, Atmos. Chem. Phys., 20, 4295–4312, https://doi.org/10.5194/acp-20-4295-2020, 2020a.

Salma, I., Vörösmarty, M., Gyöngyösi, A. Z., Thén, W., and Weidinger, T.: What can we learn about urban air quality with regard to the first outbreak of the COVID-19 pandemic? A case study from central Europe, Atmos. Chem. Phys., 20, 15725–15742, https://doi.org/10.5194/acp-20-15725-2020, 2020b.

Salma, I., Varga, P. T., Vasanits, A., Machon, A.: Secondary organic carbon and its contributions in different atmospheric environments of a continental region and seasons, Atmos. Res., 278, 106360, https://doi.org/10.1016/j.atmosres.2022.106360, 2022.